Available online at www.sciencedirect.com
ScienceDirect
Catalysis Today 130 (2008) 492–500
CATALYSIS TODAY
www.elsevier.com/locate/cattod

Low-emission diesel production by upgrading LCO plus SR diesel fractions

Roberto Galiasso Tailleur

Department of Chemical Engineering, Texas A&M University, College Station, TX 77843-3122, United States

Available online 3 December 2007

Abstract

The performance of commercial hydrotreating units that use 15% LCO/85% SRGO as feed stock and a $MoNi/Al_2O_3$-type catalyst to produce 30-ppm sulfur diesel was followed along the cycle length. The products generated at the 1st, 8th and 14th months on stream were deeply characterized to enable understanding of the changes in quality along the cycle length. Three catalyst samples at the end of run were obtained from the reactor and characterized. Furthermore, a $WNiPd/TiO_2Al_2O_3$ catalyst, deactivated in the pilot plant during 3 months in operation with 100% LCO as feedstock, was then used to process the same feedstock as in the commercial unit. A diesel engine test was done with the three products obtained along the cycle length as well as with others obtained in the pilot plant to check the effect of deactivation on emissions. The results confirmed metal and acid site deactivation, decrease of cetane number and increase in emissions along the cycle length. The test with a synthetic feed demonstrates that the metal sites on the catalysts deactivated more slowly than the isomerization and cracking ones.

Keywords: LCO; Hydrotreating; Low sulfur diesel; Cetane number; Emissions

1. Introduction

The valorization of light catalytic oil (LCO) fractions in high-pressure hydrotreating commercial units to produce a low-sulfur high-cetane diesel component is a growing area of interest. We studied different methods of upgrading low-quality (high sulfur and aromatic) middle-distillate fractions into a high-quality diesel [1]. Streams like LCO and light coker gas oil (LCGO) are increasingly produced in refineries that upgrade heavy oils. They are potential feedstocks to be processed with straight run gas oil (SRGO), but their extremely poor quality (high in sulfur and aromatics and low cetane number (CN)) limit their incorporation due to the catalyst deactivation that shortens the cycle length [2]; the degree of deactivation depends on the type of catalysts and the hydrogen partial pressure used in the unit.

A large-scale effort is currently underway to achieve the ultra-low-sulfur diesel, but still to be developed is a means to resolve the stability of the catalyst when the hydrotreating HDT unit processes a highly aromatic feedstock. Cetane number is an important product specification that depends on the degree of ''paraffinicity'' of the diesel: the lower the amount of aromatics and naphthenes, the better is the performance of the fuel in a diesel engine. Modern diesel engines, having incorporated multiple injections, EGR and post-treatment technology [3], are able to produce low NOx and PM emissions using fuel with low sulfur, low aromatics, and a high cetane number. The production of a significant volume of 15-ppm diesel has challenged refinery operation since 2006. Revamping the old (and all) HDT units and the use of advanced catalyst technology and reactor loading resolved the problem in part, but still, refineries need to limit high aromatic content feeds to assure a proper cycle length. Cetane number and cetane index (CI) are properties that can be increased to some extent by deep hydrogenation at moderate H_2 partial pressure. The LCO is a peculiar type of feed because it is produced by the cracking of heavy gas oil inside a zeolitic cage that converts some poly-alkyl-polyaromatics boiling in the range of 350–500 °C (C_{20} to C_{35}) into other poly-alkyl-polyaromatic compounds boiling in the range 180–350 °C (C_{10} to C_{20}) by cracking the paraffinic branches that surround the tri-, di- and mono-ring aromatics and naphtheno-aromatics. That accumulated in the diesel boiling range a high proportion of poly-branched aromatics (40–60 wt%) and naphtheno-aromatics (20–30 wt%) compounds with very short paraffins in branches and an extremely

E-mail address: reg2005@chemail.tamu.edu.

0920-5861/$ – see front matter © 2007 Elsevier B.V. All rights reserved.
doi:10.1016/j.cattod.2007.10.074

low cetane number. These molecules are difficult to convert into paraffins using conventional HDT catalysts. The main hindrance is the type and stability of the acid sites used. The path of polyaromatic reaction starts by their adsorption in the metallic sites where the first ring is hydrogenated quite quickly. These sites could be the traditional sulfide of W or Mo coupled with Co or Ni transition metals, or with noble metals (Pd, Pt), among others. The same sites are used to achieve the deep desulfurization throughout via direct and indirect ways [4]. Ring hydrogenations, such as the conversion of poly-alkyl-tetralin into other naphthenic cycles (for instance, poly-alkyl-decalin) is highly controlled by thermodynamic equilibrium and by the aromatic adsorption competition. The naphthenic ring opening reactions occur in series-parallel to produce a large alkyl chain branched to aromatic and naphthenic molecules. The newly formed side chains – linked to polyaromatic or naphtheno-aromatic nuclei – have higher cetane numbers than the original aromatics, but they might subsequently become cracked and dealkylated, losing the CN [5]. Pure hydrogenating reactions improve cetane number only by 2–4, while the ring opening reactions might increase cetane number by as much as 10 if paraffinic branches are preserved.

Bacaud et al. [6] demonstrated a very interesting effect of catalyst deactivation in selectivity during the hydrogenation of heavy gas oil, postulating the sintering of the active phase. Eijsbourts and van Leerman [7] reported that MoNi-type catalyst was deactivated by losing the MoS_2 dispersion. The topology (shape and size of the pores) of the catalyst is changed by coke deposition that might affect to some extent the formation of some isomers and desorption of large molecules. Muegge and Massoth [8] demonstrated that the coke deposition might reduce the effective diffusivity by pore mouth constriction, and Maraffi and Stanislaus [9], among others, that initial coke deposition modified the pore structure, surface, and volume. Bellare et al. [10] used the Arrhenius plots to determine the extent of site suppression and pore blockage. One important factor as regards this type of reaction is the number and strength of acid sites. Adsorption energy of the large alkyl-aromatics molecules depends upon the type of acid site involved, and the adsorbed species will affect surrounding metal and acid sites. In other words, the presence of large molecules adsorbed on acid sites can change the activity and selectivity of the catalyst. Maraffi and Stanislaus [11] found no correlation between the initial coke deposition and the acidity of different MoNi-type catalysts. Galiasso [12] reported that after the initial loading of coke during the hydrocracking of VGO, the cracking and ring opening reactions seem to be affected by a small amount of coke accumulation along the cycle, without additional modification in pore diffusivity. Other important work in the area of ring opening involving LCO is noted in the work of Nylen et al. [13].

The present contribution focuses on study the quality of the diesel along the cycle length when 15% LCO + 85% SRGO are processed to produce a low-sulfur medium-cetane number diesel. The main objective is to understand the relative deactivation of the catalytic sites responsible for sulfur removal, aromatics hydrogenation and ring opening reactions.

2. Experimental

2.1. Catalyst chemical characterization

The catalyst used in a commercial HDT unit was a MoNi/Al_2O_3 type. Three samples of spent catalysts were obtained from the reactor using a purpose-built device at the end of run, washed with xylene under reflux at 80 °C, and dried in nitrogen. The xylene extract was disregarded because its composition depends on the shutdown procedure. Then carbon, hydrogen and sulfur content were analyzed using Leco and plasma elemental analyzers. ''Soluble'' carbon was extracted by washing the samples for one day under reflux with carbon disulfide at 90 °C, then drying them in nitrogen. The amount of insoluble carbon was determined by Leco and characterized by FTIR and solid ^{13}C NMR. The insoluble coke was extracted from the catalyst by treating the samples with fluorhydric acid at room temperature, washing the coke with xylene and then drying it under nitrogen at 80 °C. The other catalyst was a $WNiPd/TiO_2Al_2O_3$ deactivated in a pilot plant for 3 months on stream with 100% of LCO [14]. This catalyst was selected because it was particularly suited for ring opening reactions [5]. It was characterized with the same techniques for comparison purposes.

2.2. Textural catalyst analysis

The micro- and macro-mesopore volume was measured by mercury porosimetry and by nitrogen physisorption using a Micromeritics apparatus.

2.3. Acidity measurement

Pyridine thermal desorption analysis (PTD) and the IR spectroscopy characterized the total acidity and the strength and type of acid sites in the spent catalysts before and after extraction with CS_2. A McBain microbalance and IR spectroscopy with a 1-mg sample were used. The catalyst was treated with a stream of argon (3 l/min) until constant weight was achieved using a program of 10 °C/min. to increment the temperature from 30 to 300 °C while recording the weight losses. After reaching constant weight, the temperature was kept constant at 300 °C for 2 h and then cooled down at a rate of 10 °C/min. A stream containing pyridine (0.001 molar) diluted in argon was passed through the catalyst at room temperature (30 °C) for 2 h. After that, pure argon was flowed at the same temperature for another 2 h. The amount of pyridine retained on the catalyst was measured and reported as millimols of pyridine/g. The sample was then removed under inert atmosphere and analyzed by IR spectroscopy (Nicolet, 2000, bands: Lewis at 1445 cm^{-1}; Brönstead at 1540 cm^{-1}). In another sample of the same catalyst, pyridine was adsorbed at the same operating conditions, but then the solid was heated in argon using a ramp of 6 °C/min, and the remaining amount of pyridine at 200 or 300 °C was measured (Table 1). Both samples were characterized by IR spectroscopy. The pyridine adsorption analysis gives the total acidity at 30 °C, and the ratio

Table 1
Properties of spent and reference catalysts

Catalyst (EOR)	Top (Spent 1)	Middle (Spent 2)	Bottom (Spent 3)	Reference
Pore volume (cm^3/g) AE	0.32	0.29	0.28	0.38
Micropore volume (cm^3/g) BE	0.1	0.1	0.08	0.07
Micropore volume (cm^3/g) AE	0.12	0.11	0.09	0.08
D_{effMac}–D_{effMic} (cm^2/s) × 10^4 AE	0.52–0.1	0.48–0.08	0.50–0.08	0.68–0.09
Soluble coke (wt%)	1.9	2.1	1.6	1.6
Insoluble coke (wt%) AE	5.4	5.3	5.4	5.6
$(H/C)_{CS_2}$–$(S/C)_{CS_2}$ mol ratio	1.11–0.12	1.09–0.14	1.10–0.16	1.14–0.11
$(Pyr.)_{200\ °C}$–$(Pyr.)_{300\ °C}$ (mmol/g) BE	0.017–0.015	0.015–0.012	0.014–0.01	0.03–0.01
$(I_{1540}/I_{1445})_{200\ °C}$–$(I_{1540}/I_{1445})_{300\ °C}$ BE	0.12–0	0.05–0	0.03–0	0.9–0.6
$(I_{1540}/I_{1445})_{200\ °C}$–$(I_{1540}/I_{1445})_{300\ °C}$ AE	0.15–0	0.08–0	0.09–0	1.1–0.7
Sulfur (wt%) BE	5.9	6.1	6.2	6.1
(I_{Mo}/I_{Me})–(I_W/I_{Me}) (mol/mol) BE	2.0–0	1.88–0	2.15–0	0–2.12

AE and BE denotes after and before extraction with CS_2, respectively.

of strong/weak acid sites at 300 °C is measured by mols of pyridine retained at 300 °C divided by mols released by the surface at temperatures between 200 and 300 °C. The reference catalyst was also analyzed with the same techniques.

2.4. X-ray photoelectron spectroscopy (XPS)

The XPS equipment was a Bruker 300 apparatus (Al cathode), that uses Al Kα 1486.6 eV, and with 200 W of power. For peak area measurements, a Shirley-type integral background was used. When multiple components were present under a given XPS envelope, a non-linear least-square-curve fitting routine was implemented (Levenberg–Marquardt damping method). All peaks were fitted using a Voight function with 20% Lorentzian character. Curve fitting of the W 4f region (42–32 eV) was carried out according to the methodology described by Briggs and Seah [15]. The XPS parameters (peak position, peak width) relative to W^{4+} were obtained by curve fitting the spectra of the fresh catalyst. These parameters were kept constant when fitting the spectra of spent specimens. The results were reported as relative intensity values of the metal divided by sums of metal intensities: Mo + Ni + Al or W + Ni + Al + Ti (I_{Mo}/I_{Me} and I_W/I_{Me}).

2.5. Catalyst characterization by "probe" molecules

The commercial and reference catalysts were tested using a synthetic feed containing 15,000 ppm of sulfur as dibenzothiophene, 35% of 1-methyl-naphthalene (MeN) and 10% of 1-methyl-tetralin (MeT), 5% of decalin (D) in hexadecane. The temperature was 340, 350 or 360 °C; other operating conditions were 0.5 h^{-1} of LHSV, 4 H_2/HC molar ratio and 12.5 MPa of total pressure. The products were analyzed by GC.

2.6. Effective diffusivity measurement

A shallow-bed string reactor [16] was used to measure effective diffusivity. There, seven equal-size pellets were installed in a plate in the parallel-channels of the reactor and heated to the operating temperature (120 °C). Then the inert gas (He) was flowed at 2 cm^3/s until pressure and temperature in the system were constant. The detector measuring the inlet and outlet concentration was calibrated to have a linear response at the concentration selected for the test. A pulse of benzene was injected in the chamber and the concentration output measured with fresh and spent catalyst to determine their macro- and micro-effective diffusivity using a technique developed in 1990 by Galiasso [16].

2.7. Feed and product characterization

By employing gas chromatography coupled with mass spectrometry (GC–MS) to analyze the feed and products, it was possible to determine families of aromatic, paraffinic and naphthenic compounds. The families of sulfur and nitrogen compounds were measured with the same apparatus coupled with specific GC detectors. The ^1H NMR (nuclear magnetic resonance) analysis was performed in parallel to discriminate *iso*-paraffin from *n*-paraffin in the feed and in the products. Cetane number was measured in a diesel engine using ASTM 0613 standard procedure.

2.8. Diesel engine testing of the products

The nitrogen oxide (NOx) and particulate (PM) emissions were measured in a high speed Mercedes-Benz diesel direct-injection engine operating at 1500 rpm, 150 kW power, 890 kPa BMEP and 1.130 N m. To determine NOx and PM, a micro-tunnel device coupled with on-line micro-filter and IR analyzer were used. The pressure and temperature in the chamber were recorded and soot molecular composition determined by IR. NOx, SOx, PM, CO, THC, CO_2 and soot composition were measured by triplicate.

2.9. Commercial hydrotreating operation

The performance of the commercial unit operating over a period of 1 year to produce 30-ppm diesel component was followed up by full analysis of the feed and product after 1, 8, and 14 months on stream (SOR, MOR, EOR, respectively). At these time intervals on stream, test runs were carried out controlling all operational variables. At the end of the run, the

unit was shut down under hydrogen flows and large samples of catalyst were taken from the upper, middle and bottom of the reactor beds using a purpose-built device. The samples, referred to as Spent 1, 2 and 3, were characterized under conditions permitted by the catalyst supplier.

The $WNiPd/TiO_2AL_2O_3$ catalyst was deactivated in a pilot plant (isothermal reactor) using 100% LCO as feedstock operating for 3 months with constant sulfur in the product (30 ppm). The temperature was changed along the cycle length, but the other operating conditions (P, 1/LHSV and H_2/HC ratio) were similar to those used in commercial operation.

2.10. Reaction model

A simulation model that takes into account the hydrotreating and cracking reaction network was previously developed [17]. The model is based on a large number of experimental data developed in the pilot plant using the synthetic feed and the reference catalyst. The model equations for aromatics conversion are summarized in Table 4. The model considers the presence of one metal (m) and two acid sites (a1 and a2) and incorporates the effects of hydrocarbon vaporization in the hydrogen and hydrocarbon concentrations in liquid phase (C_{H_2} and C_i), and the competitive adsorption of diaromatics (D_{DAr}), naphtheno-aromatics (K_{NAr}) and sulfur (K_{DBT}) in all sites using a LHHW type of equations. Here the model is used only to predict the change in the pre-exponential reaction rate constants ($k_{om,j}$, $k_{oa1,j}$, and $k_{oa2,j}$), which are proportional to the number of active sites, by calculating the rate constant for the different reactions at start of run and at end of run.

3. Results and discussion

3.1. Spent catalyst analysis

The textural analysis indicated that the spent catalysts at the end of run had medium macro-mesopore volume decreasing along the reactor volume. It is worth noting that the catalyst was deeply washed with xylene and does not include the aromatics adsorbed during the operation and final cooling of the reactor bed. The reference catalyst – deactivated with LCO in the micropilot plant – had 30% higher macro-mesoporosity (Table 1). In all samples the remaining microporosity and average macroporous are comparable and contain similar amount of insoluble carbon. The total carbon content follows the order middle > top > ref > bottom. The profile of carbon distribution along the bed has been already observed in two other commercial units and is attributed to an in-series mechanism of coke-precursor formation and adsorption.

The values of the benzene effective macrodifusivity (D_{effMa}) – measured in a comparative way – followed the order of the total carbon content (soluble plus insoluble; Table 1, D_{effMac}–D_{effMic}, left values): the higher the carbon, the lower is the diffusivity. In comparison, the deactivated reference catalyst had 40% higher macro-diffusivity, in agreement with its larger macro-mesopore volume. Micro-diffusivities (Table 1, D_{effMi}, right values) are quite similar for all catalysts – commercial and reference – in agreement with their similar micropore volume and coke content. The commercial and reference catalysts look similar in total micropore area and micropore difussivity, but differ in the mesopore volume and diffusivity.

Solid ^{13}C NMR analysis of the insoluble coke in commercial samples indicated a similar structure of Spent 1 (top) and Spent 3 (bottom) (end of run) (Fig. 1, spectra b and d). They present the characteristic turbostratic structure of an aged coke probably deposited at the beginning of the cycle length. They also had a similar amount of insoluble coke (Table 1, 6th row). Analysis of the soluble coke extract by CS_2 from the commercial samples shows different IR and ^{13}C NMR structure (not shown), and chemical composition. Soluble cokes are composed of condensed polyaromatics (carboide-type structure) with higher H/C molar ratio on the top of the reactor, and lower in the bottom (Table 1, 7th row, left value). The soluble coke presents the highest S/C ratio molar ratio in the Spent 2 sample (middle of the reactor; Table 1, 6th row, right value). After extraction with CS_2 all samples presented a slightly increase (~5%) in surface area and micropore volume. Based on these results, it seems that the soluble carbon might be located mainly in the microstructure. The reference catalyst, with Pd on the active phase, shows important differences in soluble coke, in contrast with the commercial catalyst. First, the reference catalyst presents a higher H/C and lower S/C molar ratio than all commercial samples (Table 1, 6th row), and shows higher aromaticity, according to the ratio of the peaks at 158/138 ppm in the ^{13}C NMR spectra, than Spent 1 and Spent 3 catalysts (comparing Fig. 1e with Fig. 1a and c). But its insoluble coke looks similar to the other samples (Fig. 1f compared with Fig. 1b and d); therefore, the difference in active sites deactivation, if any, might be mainly associated with the amount and type of "soluble" coke.

The IR analysis of the acidity for the top, middle and bottom samples was performed by adsorption of pyridine at 30 °C

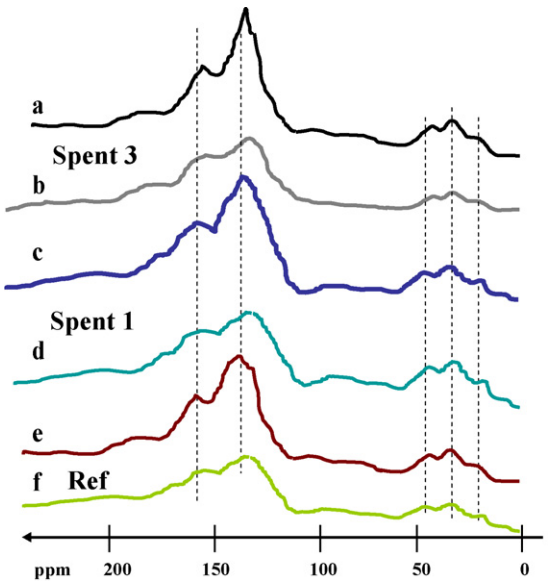

Fig. 1. ^{13}C NMR spectra of Spent 1-top (a and b), Spent 3-bottom (c and d) and reference catalyst (e and f).

before extraction (BE) and after extraction (AE) with CS_2, and desorption at 200 and 300 °C. The Spent 1 sample presented higher acidity than those of Spent 2 and Spent 3 at 200 and 300 °C (Table 1, 8th row) before extraction. Now the ratio of pyridine released between 200 and 300 °C are 0.42, 0.25 and 0.4 along the bed signaling the presence of a higher number of week acid sites on top and bottom than in the middle of the reactor. The amount of both weak acid sites is higher in the deactivated reference catalyst for a similar quantity of strong acid sites. On average, the results show that the commercial catalyst had a slightly higher proportion of strong acid sites than those of the reference. The IR analysis of those samples measuring the Lewis and Brönstead sites ratio after being desorbed at 200 and 300 °C before extraction (Table 1 rows 9, left and right values, respectively) shows large differences in the I_{1540}/I_{1445} ratio between commercial catalysts, and also between commercial and the reference catalyst. At 200 °C, the Brönstead/Lewis ratio acid is higher on top of the Spent 1 than in the bottom, but at 300 °C, the Brönstead had disappeared in all three samples. In the reference catalyst (AE), larger quantities of Brönstead sites remain at 300 °C than in commercial catalyst. After extraction with CS_2, the Brönstead/Lewis ratio increases for all samples, and the values keep a trend similar to those described before; therefore, soluble coke seems to be deposited mainly on weak and strong Brönstead type sites, and less on Lewis sites. Finally, the analysis of the accessible metal to the XPS on surface (extracted samples) indicated a medium-low concentration of Mo $3d_{5/2}$ on surface (position 228.5 eV, FWMH: 2.4) in comparison to other spent molybdenum-type HDS catalysts measured in the past. Shimada et al. [18] proposed that molybdenum sulfide moves from the alumina to the coke layer, causing the new metal structure to lose activity and selectivity, but we have no evidence of this migration. The reference catalyst lost 40% of the W $4f_{7/2}$ (position 32.3 eV, FWHM: 2.05) XPS signal. The W (XPS-accessible) metal content on surface of the reference catalyst is higher than that of molybdenum in commercial catalysts, but the change in metal concentration is not available for the latter. Total sulfur content is quite similar in both extracted samples. Nevertheless, sulfur on the surface – measured by XPS – presents two superimposed signals at 161.8 and 160.5 eV attributed to S 2p in different surroundings, one coordinated to the metal and the other to the carbon. The ratio of these two signals is 0.22 (average) for commercial catalysts and 0.44 for the reference (different metal loading). The dissolution of the Spent 1 and reference catalyst with fluorhydric acid and their analysis showed the presence of 0.1 and 0.14% of sulfur, respectively, in the insoluble cokes, which confirm the presence of sulfur in the carbonaceous structure. Having established the differences in the coke deposited on commercial samples and on the reference one, its impact on activities and selectivity will be discussed.

3.2. Product quality in commercial operation

Table 2 shows the properties of the commercial Feed 1 used during the test run and the products obtained at the SOR, MOR and EOR for commercial catalyst at constant sulfur (HDS) conversion (0.1 h^{-1}, 12.1 MPa, 4 H_2/HC molar ratio, variable temperature). The rightmost column presents the results obtained in the pilot plant with the reference catalyst and the same feedstock. The temperature required to keep around 30 ppm of sulfur in the products is indicated in the second row. The catalyst shows a clear deactivation by processing this feed, and the higher temperature was needed along the cycle length to maintain the sulfur constant in the product. The detailed analysis of the DBT and naphtho-thiophene (NT)-type sulfur can be seen in the second and third rows. The results shows a progressive increase of DBT type compounds content to the detriment of the other sulfur in the products due the different activation energy of those compounds and the different type of mechanism involved in their reaction along the cycle length. Note that desulfurization occurred via direct and indirect paths of reaction. The detailed analysis of the type of DBT compounds present in the products of both catalysts indicated a progressive increment of poly-alkylate-dibenzothiophene as a function of time on stream. It was verified in the commercial operation that at the end of run due to the average high temperature used there is no more possibility of producing 30-ppm sulfur content diesel without deteriorating further the color. The unit was shut down for this reason.

Table 2
Analysis of the product in commercial and pilot plants

Properties in wt%	Commercial feed	SOR	MOR	EOR	Reference catalyst
MWA temperature (°C)	–	340	352	370	367
DBT type of sulfur (ppm)	15,000	20	25	30	24
Naphtho-aromatic sulfur (ppm)	1,430	10	5	0	6
Diaromatics	25	10	12	14	8
Monoaromatics	15	18	18	17	13
Naphtheno-aromatic	15	10	11	12	11
Tricycloparaffins	1	1.8	2	2.2	0.5
Di-cyclo paraffins	10	16	15	14	16
Mono-cycle paraffins	15	15	16	17	21
Paraffins (wt)	20	29.2	26	23.8	30.5
C_5–C_{10} (wt%)	0	4.3	5.2	6.1	5.2
C_1–C_4 (wt%)	0	1.8	2.3	2.6	2.2
Cetane number	–	43	41	39	40

Table 2 shows an important change in hydrogenation and cracking reactions as function of time on stream. There was a different rate of deactivation of the function of metallic and acid sites on the catalytic surface. Deactivation of metallic sites is responsible for some reduction in hydrogenation capabilities. Deactivation of acid sites produces a large cutback of isomerization and ring opening reaction, responsible for increasing paraffin content. Table 2 shows increment in the wt% of diaromatics and naphthenic-aromatic molecules and small reductions in mono-aromatics, mono-naphthenes and C_{10}^{+} paraffins content, despite the increments on temperature performed along the cycle. These phenomena contribute to the decrement cetane number (diesel quality) along the cycle length at quasi constant hydrogen consumption. The isomerization and naphthenic ring opening sites are less and less able to produce poly-alkyl-benzene- and poly-alkyl-cyclohexane-type compounds – reducing the proportion of paraffin to aromatic rings in the molecules – because cracking and dealkylation reaction of the aromatic branches increase along the cycle. As a result, the intermediary compounds (naphtheno-aromatic) increase. Note that the commercially deactivated catalyst after 14 months on stream performed similarly to the reference catalyst deactivated after 3 months with pure LCO in the pilot plant. C_1–C_4 paraffins increase with the time on stream due to the increment of temperature that signals the survival of the cracking and dealkyation active sites. The ''passivation'' of the surface is not proportional to the amount of carbonaceous deposit, nor to the decline in total acidity of the sample. The deactivation seems to be more associated with the selective elimination of some type of acid sites. A mechanistic discussion about the path of reaction will be presented based on the results obtained with ''probe'' molecules.

3.3. Study of catalyst deactivation using probe molecules

At the end of run, a weight-average sample of commercial and reference catalysts was tested using a blend of 30% of methyl-naphthalene, 10% of methyl-tetralin and 15,000 ppm of sulfur as dibenzothiophene in hexadecane. The operating conditions were 340, 350 and 360 °C, 0.5 h^{-1} of LHSV, 4 H_2/HC molar ratio and 12.5 MPa of pressure. The study of the effect of temperature will distinguish between the sensitivity of the main reactions to temperature from acid site deactivation. In Table 3, the second row presents results obtained by hydrodesulfurization as a function of temperature for both catalysts. For the commercial catalyst in presence of diaromatics, the dibenzothiophene (DBT) is mainly desulfurized into phenylbenzene following the direct route for sulfur removal, in agreement with previous results [2,17]. The competitive effect of diaromatics in desulfurization reduced the indirect route that produces cyclohexylbenzene as main product. The phenylbenzene might be also hydrogenated to produce phenylcychohexane, but the detailed analysis of the products indicated that the latter compound was scarcely formed at the temperature considered here for the commercial catalyst. The selectivity to direct route desulfurization is lower for the reference catalyst (70%) than for the commercial one (85%). This fact is due to the different concentration and type of metal exposed on surface, and the presence of noble metal in the former catalyst.

Table 3 shows that both catalysts are still able to convert MeN into MeT and then into decalin in a consecutive reaction using the remaining metal sites. But both catalysts had difficulty converting these two products into alkyl-benzene and alkyl-cyclohexane compounds on the acid sites. The latest reactions are responsible for the shift in the hydrogenating equilibrium and the production of more ''paraffinic'' type molecules. Hydrogenation reaction rate in the commercial samples experienced a modest rise with the temperature in comparison to those observed with the reference catalyst due again to the presence of noble metal in the latter.

To analyze the effect of ring opening reaction deactivation, the performance of the reference catalyst is considered first. A kinetic model was previously developed using a set of 240 experimental results [17] for the same fresh catalyst and synthetic feed. Table 4 summarizes the equations used for

Table 3
Test of spent catalysts with synthetic feed (0.5 h^{-1}, 12.5 MPa, 4 (molar) H_2/HC)

Catalyst	Commercial			Reference		
Temperature (°C)	340	350	360	340	350	360
Sulfur (DBT) (ppm)	350	70	30	450	88	37
Cyclo-hexyl-benzene (wt%)	0.1	0.3	0.5	0.3	0.6	1.1
Naphthalene (all) (wt%)	15.8	16.6	17.1	13.9	12	11
Tetralin (all) (wt%)	12.5	11.2	10.8	11.7	10	10.5
Decalin (all) (wt%)	5.4	4.9	4.7	7.01	8.6	9.3
Alkyl-benzene (all) (wt%)	1.4	1.7	1.5	3.4	3.6	2.4
Alkyl-cyclohexane (all) (wt%)	1.4	1.3	1.1	1.1	1.2	0.8
Benzene (wt%)	0.5	0.9	1.8	<0.1	0.2	0.6
Cyclohexane (wt%)	<0.1	0.2	0.3	<0.1	0.5	0.6
Conversion nC_{16} (wt%)	19	26	32	25	35	47
C_3–C_4 (wt%)	5.1	9.1	12.2	6.2	12.3	17.8
C_7 (wt%)	3.4	2.8	2.3	6.3	4.8	4.2
C_8 (wt%)	5.2	4.3	3.8	7.7	7.1	6.4
iC_7/nC_7 (wt)	0.5	0.6	0.7	0.7	0.84	0.93
iC_8/nC_8 (wt)	0.72	0.88	0.92	0.82	1.1	1.25

Table 4
Reaction model for the hydrogenation of MeN and MeT

$$-R_{m,MeN-MeT} = \frac{k_{m1} C_{MeN} C_{H_2}^2}{1 + K_{mDAr} C_{DAr} + K_{mNAr} C_{NAr} + K_{mDBT} C_{DBT}} \quad (1)$$

$$R_{m,MeT-MeD} = \frac{k_{m2} C_{MeT} C_{H_2}^3}{1 + K_{mDAr} C_{DAr} + K_{mNAr} C_{NAr} + K_{mDBT} C_{DBT}} \quad (2)$$

$$R_{a1,MeT-DMeI} = \frac{k_{m3} C_{MeT}}{1 + K_{a1DAr} C_{DAr} + K_{a1NAr} C_{NAr} + K_{a1DBT} C_{DBT}} \quad (3)$$

$$R_{a1,MeD-DMNN} = \frac{k_{a1,4} C_{MeD}}{1 + K_{a1DAr} C_{DAr} + K_{a1NAr} C_{NAr} + K_{a1DBT} C_{DBT}} \quad (4)$$

$$R_{a1,DMeI-PB} = \frac{k_{a1,5} C_{DiMeI}}{1 + K_{a1DAr} C_{DAr} + K_{a1NAr} C_{NAr} + K_{a1DBT} C_{DBT}} \quad (5)$$

$$R_{a2,PB-B} = \frac{k_{a2,6} C_{PB}}{1 + K_{a2DAr} C_{DAr} + K_{a2NAr} C_{NAr} + K_{a2DBT} C_{DBT}} \quad (6)$$

$$R_{a1,DMeNN-PCH} = \frac{k_{a1,7} C_{DiMeNN}}{1 + K_{a1DAr} C_{DAr} + K_{a2NAr} C_{NAr} + K_{a1DBT} C_{DBT}} \quad (7)$$

$$R_{a2,PCH-CH} = \frac{k_{a2,8} C_{PCH}}{1 + K_{a2DAr} C_{DAr} + K_{a2NAr} C_{NAr} + K_{a2DBT} C_{DBT}} \quad (8)$$

$$-R_{m,PB-PCH} = \frac{k_{m,9} C_{PB} C_{H_2}^3}{1 + K_{mDAr} C_{DAr} + K_{mNAr} C_{NAr} + K_{mDBT} C_{DBT}} \quad (9)$$

$$-R_{m,B-CH} = \frac{k_{m,10} C_B C_{H_2}^3}{1 + K_{mDAr} C_{DAr} + K_{mNAr} C_{NAr} + K_{mDBT} C_{DBT}} \quad (10)$$

calculating the rates of aromatics conversion into paraffins. Here, the kinetic rate constants of the model k_{m1} and k_{m2} are used for the hydrogenation reactions (Eqs. (1) and (2)) that is carried out on metal site; $k_{a1,3}$ to $k_{a1,6}$ are the ring opening rate constants (Eqs. (3)–(6)) that occurred in weak acid site; $k_{a2,7}$ and $k_{a2,7}$ are the rate contant for the cracking and dealkylkation reactions (Eqs. (7) and (8)), that happened on the strong acid site. A genetic algorithm was used to calculate the value of the rate constants that predict the product distribution with less than 1% error. The constant calculation was done using the experimental data obtained at 340, 350 and 360 °C for fresh catalyst and for the pilot plant deactivated catalyst (reference).

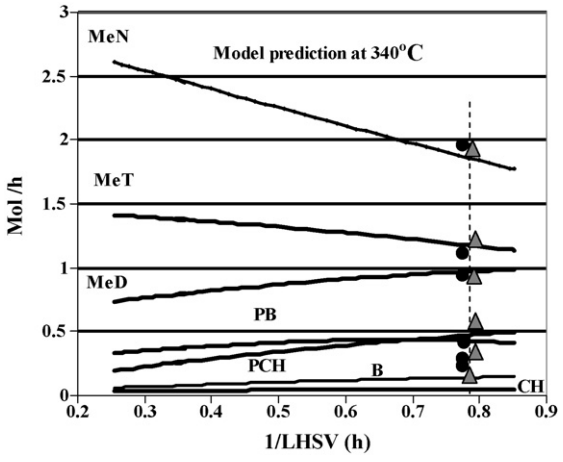

Fig. 2. Model prediction of the aromatics hydrogenation (spent-reference catalyst) and experimental points.

Fig. 1 shows, as an example, the model prediction of the mass flow rate of the compounds along the reactor for the main species (all isomers are included in the definition) present in the synthetic products (340 °C—deactivated catalyst). MeN and MeT are converted into methyl-decaline (MeD), phenylbenzene (PB), alkyl-cyclohexane (PCH), benzene (B) and cyclohexane (CH). Two sets of experimental data (flow rate values) at the reactor outlet are indicated by triangles and circles in Fig. 2. The change in the pre-exponential factor can be calculated for all the reactions assuming that the same types of sites are involved in fresh and used catalyst, thus reaction rates have the same activation energies, but the number of sites decreases with time on stream:

$$k_{ij} = k_{oij} \exp\left(\frac{E_i}{RT}\right);$$

$$\Delta k_{oij} = k_{oi,j\,\text{fresh}} - k_{oi,j\,\text{deactivated}} : \; 1.3 = \frac{\text{Isom}\,\Delta k_{o\text{MeT}-\text{DMeI}}}{\text{Hyd}\,\Delta k_{o\text{MeN}-\text{MeT}}};$$

$$1.5 = \frac{\text{Dealk}\,\Delta k_{o\text{PB}-\text{B}}}{\text{Hydr}\,\Delta k_{o\text{MeN}-\text{MeT}}}; \qquad 1.45 = \frac{\text{Dealk}\,\Delta k_{o\text{PCH}-\text{CH}}}{\text{Hydr}\,\Delta k_{o\text{MeN}-\text{MeT}}}$$

The value of the ratios shows that the most affected reaction rate is the dealkylation, followed by the isomerization of the C_6 into C_5 cycle paraffin, which is supposed to be the controlling step of the ring opening reactions [17,19]. Thus, when the temperature increases, the deakylation reaction grows faster than isomerization and ring opening, and the production of ring-open products decreases because they were preferentially dealkylated into benzene and cyclohexane. This effect contributes to the cetane number reduction. Now for the commercial catalyst, the trend seems to be more pronounced, and the experimental data (Table 3) indicates an important reduction in ring opening reaction and higher dealkylkation, than those presented by the reference catalyst. That is in agreement with the higher amount of strong acid sites shows by the former catalysts. The spent commercial catalyst is so different from the reference that the kinetic model developed for the NiMo catalyst is not able to properly predict the yield of hydrogenated product by adjusting only the k_{oij} constant, but the trend in sites deactivation seems to be similar: a2: dealkylkation > a1: isomerization and ring opening > m: hydrogenation.

In addition, the increase in temperature improves the cracking of nC_{16} for both catalysts, with a more pronounced effect in reference than in commercial sample, in accordance with the larger number but strong acid sites remaining in the former.

C_3–C_5 hydrocarbon production is boosted by increasing the temperature on deactivated samples (Table 3). The detailed analysis of the *iso*- and *n*-paraffins generated by cracking of nC_{16} is important to the understanding of deactivation of both the weak and strong acid sites. The cracking of paraffins starts by the conversion of the *n*-paraffins (n-P_j) into an olefinic intermediary (o-P_j) that is followed by an in-series isomerization into mono-, di- and tri-branched intermediaries (io-P_j = iio-P_j = iio-P_j; j being the carbon number) on weak acid sites (a1). The latter intermediaries are desorbed and then adsorbed either in a

nearby metal site or in strong acid site in competition. In this way, the intermediaries can be hydrogenated on metal sites to produce isomers (i-P_j) or cracked on acid sites to generate – after hydrogenation – lower-molecular-weight n-paraffins and isoparaffins ($iP_{j/p}$ and $nP_{j/p}$: mainly C_6–C_{11}). Then, the reactions network restarts by converting these products into other olefinic intermediaries that lead into other isomers or lower molecular weight paraffins (C_3–C_4). The light paraffins (C_3–C_4) might be produced by cracking of the alkyl-benzene and alkyl-cyclohexane and the n-C_{16}. But, the production of iC_7 and iC_8 paraffins are mainly produced by isomerization, primary cracking of C_{16} paraffin, and by ring opening. Even when, the ring opening reaction of alkyl-cyclohexanes could produce some C_7–C_{11} paraffins, their reaction rates are extremely low in presence of aromatics [17], as it can be seen in Table 3. The cyclohexane (CH) ring opening produces only C_6 paraffins. Thus it can be considered that the ratio of *iso*/*n*-C_7 and *iso*/*n*-C_8 paraffins is mainly representative of the ability of the acid sites to produce isoparaffins from C_{16}.

Table 3 shows that C_7 and C_8 *iso*/*n*-paraffin ratios are lower than 1 and increase slightly as a function of temperature for both catalysts. In parallel, the total amount of C_7 and C_8 decreases slightly as a function of temperature, while the amount of C_3–C_4 increases at much higher rate than the increase in *iso*/*n*-paraffin ratio and the yields of C_7–C_8 total paraffins. The primary cracking of nC_{16} generated a distribution of products centered at C_8 carbon number, but then the products can be isomerized into *iso*C_8 (a1) and cracked (secondary) into lighter product (C_3–C_4) paraffins (a2). The results indicated that temperature favors more the primary and secondary cracking than the *iso*C_7 and *iso*C_8 production, in spite of the slight increase observed in the *iso*/*n* ratio. This condition exists while the product distribution is not controlled by the isomerization rate of reaction in the weak acid site or by the rate of hydrogenation in the metal sites. Since the number of weak acid sites used for the isomerization is less reduced than those of strong acid sites used for cracking, the total amount of C_7–C_8 formed is driven by the strong acid sites. At higher temperatures, due to the higher activation energy of the cracking reaction (∼18 kcal/mol) than those of the isomerization (∼13 kcal/mol), an increment in cracking is observed that dominates the path of reaction in spite of the reduction on strong acid sites numbers. The previously mentioned model shows a similar trend in the change by coking of the pre-exponential rate constants of paraffin conversion compared with those observed for aromatics reactions. The survival of the alkyl-compound and the heavy paraffins formed is lower in the commercial than in the reference catalyst (ratio of benzene production per unit of diaromatics converted, and C_3–C_4 produced per unit of C_{16} converted). Therefore, the commercial catalyst seems to have low resistance to coke deactivation due to the absence of noble metal to protect the weak acid sites. The low alkyl-benzene, alkylcyclohexane production, as well the high C_3–C_4 paraffins generation, confirm that in the commercial catalyst, the main acid function that improves quality, cetane number, is deactivated at the end of cycle. The reference catalyst performance indicates the need to balance weak and strong acid sites to improve ring opening reactions and catalyst stability.

3.4. Effect of SR + LCO hydrotreatment in diesel engine emissions

The specialized literature [20–22] indicates some dependency of exhaust gas emissions on cetane number in heavy-duty diesel engines. Nevertheless, the fuel properties' impact on emissions is a controversial matter: in our previous study with HDT of LCO [23], we observed an important effect of the types of aromatics and their distribution along the boiling range in the emissions for different hydrogenation severities. The results of research for present paper indicate the impact of catalyst deactivation in NOx and PM emissions. The above-mentioned samples at start, middle and end of run were tested in a diesel engine to evaluate their emissions. The NOx and PM emissions were measured in a high-speed Mercedes-Benz LD Diesel (2002) direct-injection engine operating at the conditions mentioned in Table 5. Octyl cetane number improver was added to enable the feed to run the engine in the ''acceptable'' range of emissions (CN > 42). The injection time was optimized using a ultra-low sulfur diesel ULSD for minimum NOx emission.

The tests done at average speed and load shows that the lowest emission is produced by the start-of-run product (lower total aromatics and mono-ring-aromatics; Table 2). When the fuel is injected into the chamber after the engine is cranked, the liquid is atomized and the ignition begins. In this phase, called uncontrolled burning or flame-propagation period, most of the PM precursors are formed by thermal cracking in which the aromatics play an important role. Then the second phase starts with full combustion, resulting in peaks of pressure and temperature. From that point on, most of the NOx formed is associated with the maximum temperature attained. The pressure-volume curve measured in the engine chamber for the SOR product is flatter than that for the EOR products. This shape of the curve is associated with an earlier (and better) vaporization and a lower maximum temperature for the SOR-HDT product. Deactivation of the catalyst clearly led to higher NOx and PM (Table 5). The reference product generated better NOx and similar particulates than, for example, the MOR product, probably due to the higher content of mono-aromatics in the light part (180–220 °C), and a larger paraffinicity in the heavy part of the diesel (300–360 °C) [23].

Table 5
Diesel engine emission (Mercedes-Benz OM61 CIDI, No EGR, 1500 rpm, load 200 kPa BMEP)

Diesel/emissions	SOR	MOR	EOR	Reference
Cetane number*	46	44	42	43
NOx	6	8	14	3
PM	0.21	0.32	0.52	0.33

*To increase 2 cetane numbers, the octyl additive was added in all samples.

4. Conclusion

The commercial experience of treating LCO and SRGO with a MoNi/Al2O3-type last-generation catalyst to produce ultra-low sulfur diesel had shown an important catalyst deactivation associated with the presence of LCO in the feedstock. This deactivation is partially compensated for by increasing the weight average temperature to maintain constant the amount of sulfur in the product; nevertheless, the amount of aromatics and the diesel engine emissions increase and cetane number decreases along the cycle length. The analysis of the catalyst confirmed that the cause is the faster rate of loss of week acid sites in comparison with the strong acid and metal sites deactivation. The use of probe molecules to test the sites activity coupled with the acidity and metal dispersion analysis indicated a progressive loss in ring-opening capabilities. The sites deactivation is less pronounced in the reference catalyst due to the presence of well dispersed noble metal, which ''protects'' some acid sites, than in commercial catalyst.

Acknowledgements

The author would like to acknowledge the experimental work of Engineers J. Patrelli and B. Coresi, the advice of the Department of Mechanical Engineering of the Polytechnic University of Valencia, Spain, and the valuable discussions of Dr. Jacoviski about diesel engine testing.

References

[1] R. Galiasso Tailleur, Diesel options to meet future US and European specification, in: International Congress on Chemical Engineering, Melbourne, (2001), p. 13.
[2] R. Galiasso Tailleur, Diesel upgrading into a low emission fuel, Fuel Process. Technol. 87 (9) (2006) 759–767.
[3] EPA report, The effect of cetane number increase due to additive on NOx emissions from Heavy-Duty Highway Engines EPA420-R-03-002, February 2003.
[4] M. Houalla, D.H. Broderick, A.V. Sapre, N.K. Nag, V.H.J. De Beer, B.C. Gates, H. Kwart, Hydrodesulfurization of methyl-substituted dibenzothiophenes catalyzed by sulfided cobalt-molybdenum/alumina, J. Catal. 61 (2) (1980) 523–527.
[5] B.H. Cooper, B.B.L. Donnis, Aromatics saturation of distillates. An overview, Appl. Catal. A: Gen. 137 (1996) 203–223.
[6] R. Bacaud, S. Gamez, M. Vrinat, Aging of industrial hydrotreating catalyst, in: Preprint 230th ACS Division of Petroleum Chemistry, vol. 50/4, 2005, 375–377.
[7] S. Eijsbourts, G.C. van Leerman, Evolution of the active phase during the deactivation and regeneration of sulfidic hydrotreating catalyst, Bulletin des Societes Belges 104 (4/5) (1995) 347–352.
[8] B.D. Muegge, F.E. Massoth, Basic studies in deactivation of hydrotreating catalyst by coke, Fuel Process. Technol. 29 (1/2) (1991) 19–30.
[9] M. Maraffi, A. Stanislaus, Studies of hydrotreating catalyst deactivation by coke deposition: influence of feedstock quality on initial coking, in: Preprint 214th ACS Meeting, Las Vegas, NV, (1997), p. 11.
[10] A. Bellare, A. Raje, D.B. Dadydburjor, The constant parameter Arrhenius plot in coking and poisoning, Stud. Surf. Chem. Catal. 68 (1991) 227–234.
[11] M. Maraffi, A. Stanislaus, Influence of catalyst acidity and feedstock quality on hydrotreating catalyst deactivation by coke deposition, Petroleum Sci. Technol. 19 (5/6) (2001) 697–710.
[12] R. Galiasso Tailleur, Effect of catalyst deactivation in mild hydrocracking reactions, Comput. Chem. Eng. 29 (11/12) (2005) 2404–2419.
[13] U. Nylen, L. Sassu, S. Melis, S. Jaras, M. Boutonnet, Catalytic ring opening of naphthenic structures. Part I. From laboratory catalyst screening via pilot unit testing to industrial application for upgrading LCO into a high quality diesel blending component, Appl. Catal. A: Gen. 299 (2006) 1–13.
[14] R. Galiasso Tailleur, $WNiPd/TiO_2Al_2O_3$ catalyst deactivation during the upgrading of LCO, Fuel, in press.
[15] D. Briggs, M.P. Seah (Eds.), Practical Surface Analysis by Auger and X-ray Spectroscopy, John Wiley, 1987, pp. 511–532.
[16] T.R. Galiasso, Mass transfer in the pores deactivated by Coke, Preprint of the LACTYM Congress held in Caracas, April 2004.
[17] T.R. Galiasso, Kinetics model for n-C_{16} hydrocracking in presence of diaromatics and DBT, Ind. Eng. Chem. Res. Dev., in press.
[18] H. Shimada, T. Sato, Y. Yoshimura, A. Nishijima, S. Kashiwava, K. Ogino, An XPS study on deactivation mechanism of molybdenum catalyst for heavy hydrogen processing, X-sen Bunseki no Shinpo 18 (1987) 213–222.
[19] M. Santikupan, J. Herrera, S. Jongpatiwut, D. Resasco, Ring opening of decalin and tetralin on HY and Pt/HY zeolite catalysts, J. Catal. 228 (2004) 100–113.
[20] A. Ohtsuka, K. Hashimoto, Y. Akutsu, M. Arai, M. Tamura, Effects of cetane number and fuel properties on diesel-exahust emissions, J. Jpn. Petroleum Inst. 45 (1) (2002) 24–31.
[21] C.S. Sluder, R. Wagner, S. Lewis, J. Storey, Fuel properties effects on emissions from high efficiency clean combustion in a diesel engine, in: Society of Automotive Engineers (Special Publications) SP2012, 2006, 101–110.
[22] T. Nakajima, S. Sasali, A. Kawai, K. Akijama, Sh. Kobayashi, K. Sakamoto, Effects of fuel properties on diesel exhaust emissions. 2. Effect of aromatics of fuel on character of particulate matter and semi-volatile matter in exhaust gases, Taiki Kankyo Gakkaishi 33 (4) (1998) 262–271.
[23] R. Galiasso Tailleur, Low emission diesel production in a mild-hydrocracker that use a gas phase reactor, in: Preprint of 7th World Congress of Chemical Engineering, Glasgow, United Kingdom, (2005), pp. 10–14.